

AD-A126 611

F2 BOUNDARY LAYER MEASUREMENT IN A CHEMICAL LASER SLIT

1/1

NOZZLE FLOW. (U) AEROSPACE CORP EL SEGUNDO CA

AEROPHYSICS LAB D J SPENCER ET AL. 15 FEB 83

UNCLASSIFIED

TR-0083(3930-01)-2 SD-TR-83-09

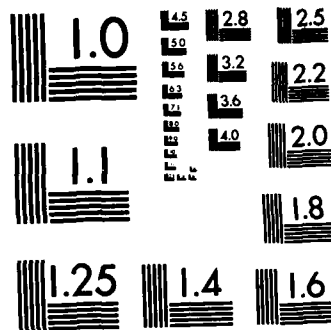
F/G 20/5

NL



END





MICROCOPY RESOLUTION TEST CHART  
NATIONAL BUREAU OF STANDARDS-1963-A

ADA 126611

12

Report SD-TR-83-09

## F<sub>2</sub> Boundary Layer Measurement in a Chemical Laser Slit Nozzle Flow

D. J. SPENCER, D. A. DURRAN,  
H. A. BIXLER, and R. L. VARWIG  
Aerophysics Laboratory  
Laboratory Operations  
The Aerospace Corporation  
El Segundo, Calif. 90245

15 February 1983

APPROVED FOR PUBLIC RELEASE;  
DISTRIBUTION UNLIMITED

DTIC FILE COPY

DTIC  
SELECTED  
APR 11 1983  
A

Prepared for  
SPACE DIVISION  
AIR FORCE SYSTEMS COMMAND  
Los Angeles Air Force Station  
P.O. Box 92960, Worldway Postal Center  
Los Angeles, Calif. 90009

83 04 08 046

This report was submitted by The Aerospace Corporation, El Segundo, CA 90245, under Contract No. F04701-82-C-0083 with the Space Division, Deputy for Technology, P.O. Box 92960, Worldway Postal Center, Los Angeles, CA 90009. It was reviewed and approved for The Aerospace Corporation by W. P. Thompson, Director, Aerophysics Laboratory. 1st Lt Steven G. Webb, Det 1, AFSTC, was the project officer for Mission-Oriented Investigation and Experimentation (MOIE) Program.

This report has been reviewed by the Public Affairs Office (PAS) and is releasable to the National Technical Information Service (NTIS). At NTIS, it will be available to the general public, including foreign nations.

This technical report has been reviewed and is approved for publication. Publication of this report does not constitute Air Force approval of the report's findings or conclusions. It is published only for the exchange and stimulation of ideas.

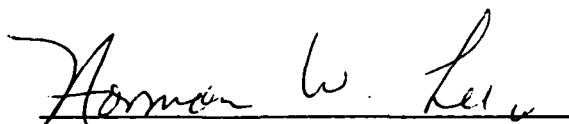


Steven G. Webb, 1st Lt, USAF  
Project Officer



David T. Newell, Lt Col, USAF  
Actg Dir Space Systems Technology

FOR THE COMMANDER



Norman W. Lee, Jr., Colonel, USAF  
Commander, Det 1, AFSTC

UNCLASSIFIED

SECURITY CLASSIFICATION OF THIS PAGE (When Data Entered)

REPORT DOCUMENTATION PAGE		READ INSTRUCTIONS BEFORE COMPLETING FORM
1. REPORT NUMBER SD-TR-83-09	2. GOVT ACCESSION NO. AD-A126611	3. RECIPIENT'S CATALOG NUMBER
4. TITLE (and Subtitle) F <sub>2</sub> BOUNDARY LAYER MEASUREMENT IN A CHEMICAL LASER SLIT NOZZLE FLOW		5. TYPE OF REPORT & PERIOD COVERED TR-0083(3930-01)-2
		6. PERFORMING ORG. REPORT NUMBER
7. AUTHOR(s) D. J. Spencer, D. A. Durran, H. A. Bixler, R. L. Varwig		8. CONTRACT OR GRANT NUMBER(s) F04701-82-C-0083
9. PERFORMING ORGANIZATION NAME AND ADDRESS The Aerospace Corporation El Segundo, Calif. 90245		10. PROGRAM ELEMENT, PROJECT, TASK AREA & WORK UNIT NUMBERS
11. CONTROLLING OFFICE NAME AND ADDRESS Space Division Air Force Systems Command Los Angeles, Calif. 90009		12. REPORT DATE 15 February 1983
		13. NUMBER OF PAGES 23
14. MONITORING AGENCY NAME & ADDRESS (if different from Controlling Office)		15. SECURITY CLASS. (of this report)  Unclassified
		15a. DECLASSIFICATION/DOWNGRADING SCHEDULE
16. DISTRIBUTION STATEMENT (of this Report)  Approved for public release; distribution unlimited.		
17. DISTRIBUTION STATEMENT (of the abstract entered in Block 20, if different from Report)		
18. SUPPLEMENTARY NOTES		
19. KEY WORDS (Continue on reverse side if necessary and identify by block number) Chemical Lasers F <sub>2</sub> Boundary Layer F <sub>2</sub> Absorption Slit Nozzle Characteristics		$\delta = 0.1(5x \cdot 100^2 \cdot x)$
20. ABSTRACT (Continue on reverse side if necessary and identify by block number) A sensitive F <sub>2</sub> absorption diagnostic suitable for slit nozzle scanning was developed and applied to the measurement of an F <sub>2</sub> boundary layer in an HF chemical laser flow. The F <sub>2</sub> boundary layer profile was determined to be of exponential decay form with peak at the nozzle wall and of width ~1/3 the viscous boundary layer. The F <sub>2</sub> concentration profile was displaced inwardly and slightly compressed by the H <sub>2</sub> slit injection at the nozzle exit plane, which penetration profile followed the relation $\delta = 0.1\sqrt{x}$ . The F <sub>2</sub> profile apparently remains fairly intact in passing through the lasing zone.		

DD FORM 1473  
(FACSIMILE)UNCLASSIFIED  
SECURITY CLASSIFICATION OF THIS PAGE (When Data Entered)

CONTENTS

I. BACKGROUND..... 5

II. EXPERIMENTAL SETUP..... 9

III. RESULTS..... 21

IV. SUMMARY..... 27

REFERENCES..... 29

DTIC  
COPY  
INSPECTED  
2

Accession For	
NTIS GRA&I	<input checked="" type="checkbox"/>
DTIC TAB	<input type="checkbox"/>
Unannounced	<input type="checkbox"/>
Justification	
Distribution/	
Availability Codes	
Avail and/or	
Special	
A	

## FIGURES

1.	Sensitive $F_2$ absorption technique schematic.....	6
2.	Experimental array used in measurements across jet.....	10
3.	Slit nozzle $F_2$ absorption scanning experiment.....	10
4.	Probe laser beam geometry along slit nozzle length.....	13
4b.	$TEM_{00}$ Gaussian intensity profile transverse to propagation direction.....	13
5.	Beam end waist, $W'$ and beam center waist, $W_{02}$ versus lens focal length.....	14
6.	Detail cross section drawing of slit nozzle array.....	16
7.	Slit nozzle flow pattern.....	17
8.	Slit nozzle $F_2$ absorption scan along 0.050 inch line for ( $H_2$ ON) and ( $H_2$ Off) conditions.....	22
9.	Measured $F_2$ density profiles (relative units).....	24

## I. BACKGROUND

The presence of recombined  $F_2$  in the boundary layers of chemical laser nozzle flows has been considered to be a source of laser inefficiency.<sup>(1,2)</sup> This inefficiency was thought to derive from (1) the reduction of F atom concentrations that contribute to lasing, (2) the inhibition of  $H_2$  mixing with the F atoms, and (3) the deleterious temperature rise produced in the flow by H atom reactions with  $F_2$ . The uncertainties in the magnitudes and distributions of the  $F_2$  molecules in the nozzle flows have hampered modeling of chemical laser performance based on this assumption, however. In response to this situation, a sensitive  $F_2$  absorption diagnostic was developed capable of detecting fractions of a percent of the associated F atom concentrations in the flows. This diagnostic device has been used in the past to probe the flows of arc-driven  $SF_6$  and  $F_2$ <sup>(3)</sup> and combustor-driven  $F_2$ <sup>(4)</sup> chemical laser nozzle flows, and to establish their total  $F_2$  recombination operational levels. Fig. 1 is a system schematic of the technique employed in these past studies. A Liconix Model 301M HeCd intracavity acousto-optic modulated laser operating at 325 nm was employed to probe the  $F_2$  concentrations in the absorption measurement region. The difference between the probe beam and reference beam intensities was measured with two independent silicon photovoltaic detectors and displayed on an oscilloscope for conditions of  $F_2$  present or  $F_2$  absent from the measurement region. The laser was square wave modulated at  $\sim 20$  Hz by an Interstate Electronics Model 125 pulse generator. The pulse generator also provides an external sync signal for the Tektronix Model 545 scope, which has a Tektronix Model 1A7A 10- $\mu$ V sensitivity differential plug-in

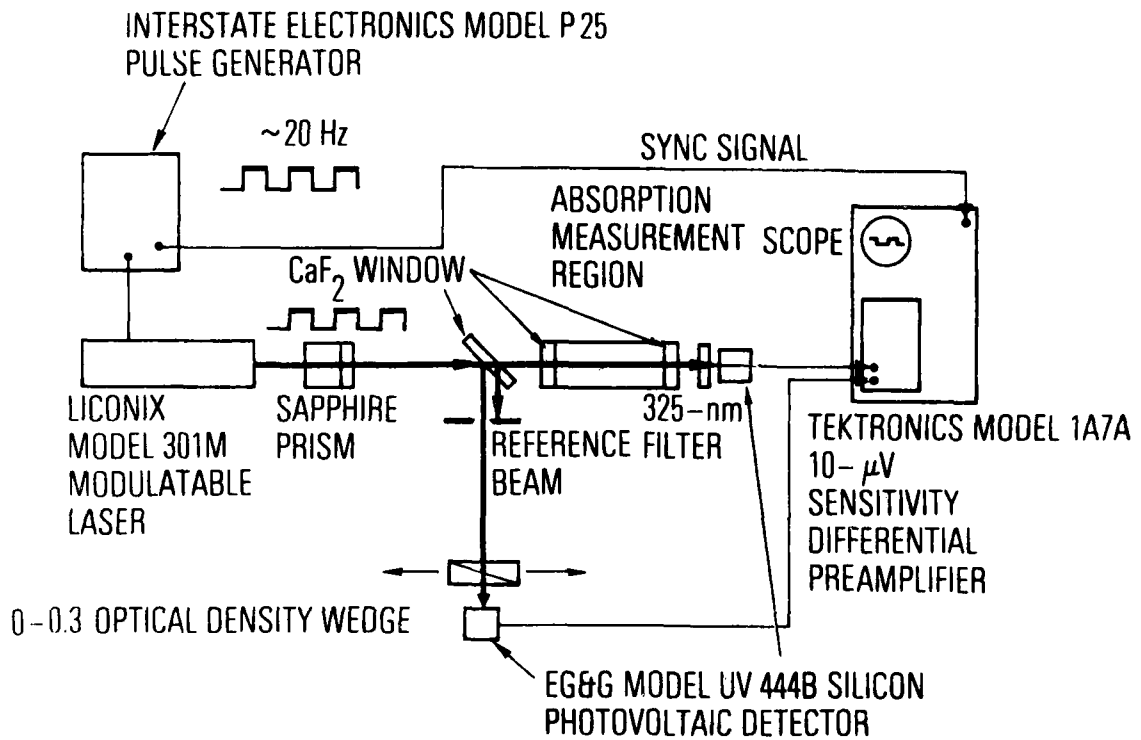


Fig. 1. Sensitive  $F_2$  absorption technique schematic

amplifier. The modulated laser beam is passed through a sapphire prism before beam splitting at a  $\text{CaF}_2$  window to eliminate the weak horizontally polarized beam from the optical path.

A narrowband 325 nm wavelength optical filter discriminates against measurement by the probe beam detector of other wavelengths generated in the absorption measurement region. An optical density wedge is used for refined intensity variation of the reference beam to obtain zero differential signal between the probe and reference beams, as measured on two EG and G Model UV 444B silicon photovoltaic detectors, for the condition of no  $\text{F}_2$  in the measurement region.

The differential intensity measurement  $\Delta I$  made upon  $\text{F}_2$  addition to the measurement region, coupled with the probe beam initial intensity measurement  $I_0$  and the absorption path length  $L$ , allows calculation of the  $\text{F}_2$  density directly from the equation

$$\rho_{\text{F}_2} \text{ (mole/l)} = (1/8.70 L \text{ (cm)}) (\Delta I/I_0) \quad (1)$$

For further details of this measurement method, see Refs. (3) and (4).

## II. EXPERIMENTAL SETUP

In the present study, a 15 mW Liconix Model 405V (UV) laser was employed to increase signal-to-noise ratio and provide a  $TEM_{00}$  beam for reduced beam size. (The model 301M laser operates at 1 mW on the  $TEM_{01}$  mode.) The  $F_2$  diagnostic was used for measurements across the entire nozzle array jet to verify the diagnostic prior to the more complex slit nozzle scanning tests. In addition, measurements across the jet near the nozzle exit plane and 1-1/2 inches downstream were made to establish the total  $F_2$  loss in passage through the jet. A photograph of the experimental array as used in absorption measurements across the jet is shown in Fig. 2. The  $F_2$  absorption diagnostic was modified to provide 0.006 inch diameter resolution over a 1-1/2 inch path length for scanning of slit nozzle flows to determine the  $F_2$  boundary layer profile. The modifications consisted of adapting the probe beam to the geometrical constraints imposed on the experiment by the slit nozzle flow. Details of the absorption measurement region for the slit nozzle  $F_2$  absorption scanning experiment are shown in Fig. 3. The drawing orientation allows one to view the vertically oriented slit nozzle array from a position downstream along the flow axis. The 18 inch square test section enclosure is shown crosshatched with 9 inch windows at cutouts on the sides and top. The probe beam from the laser on the right enters the test section horizontally through the 14 inch focal length quartz lens and a vacuum sealed  $CaF_2$  window. A first surface folding mirror oriented at  $45^\circ$  within the test section directs the beam upward past the slit nozzle array through a vacuum sealed  $CaF_2$  window to the translatable 325 nm filter-detector assembly mounted on top of the test

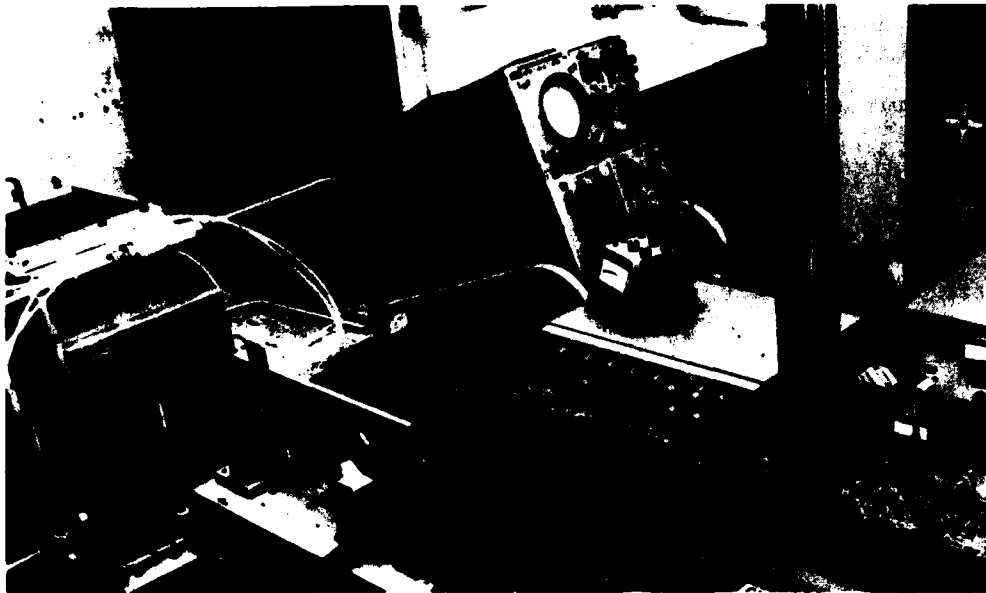


Fig. 2. Experimental array used in measurements across jet

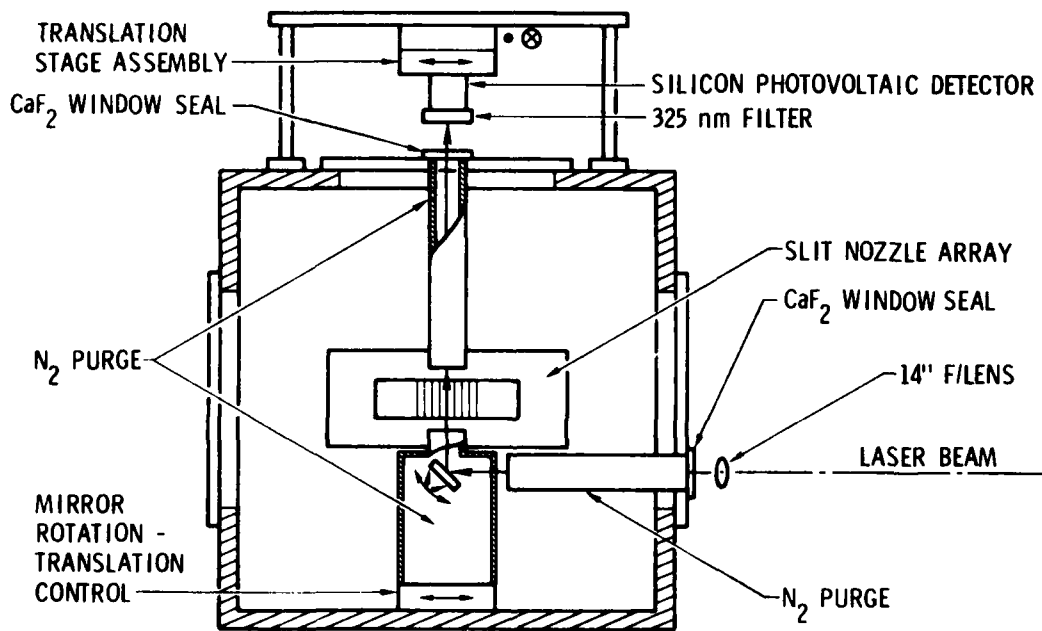


Fig. 3. Slit nozzle F<sub>2</sub> absorption scanning experiment

section. The 45° folding mirror is mounted on a translation stage controllable from outside the test section via flexible coupling cable for micrometer movement across the jets. In addition, the mirror mount provides the mirror with two degrees of freedom rotational alignment capability. The mirror housing and ducts along the optical path are positioned within 1/8 inch of the jet and purged with N<sub>2</sub> so as to confine the measurement distance to the slit nozzle length. Intensity sensitivities of  $\Delta I/I_0 = 3 \times 10^{-5}$  were obtained with this system. This detection sensitivity corresponds to a lower limit measurability of ~ 15 milli Torr F<sub>2</sub> at T ≈ 300°K over the 1-1/2 inch absorption path length of this experiment. Beam alignment parallel to the nozzle slits was made within half a beam diameter (~ 0.003 inch displacement at nozzle blade top relative to bottom). Beam displacement from the nozzle exit plane was made with the aid of calibration shims and was also true within about a half-beam diameter displacement, top to bottom. Translation of the 45° mirror results in a scanning of the vertical probe beam across a one dimensional slit nozzle flow. The detector also requires translation to maintain the probe beam signal at maximum sensitivity for the differential measurement. In tests the beam was positioned with respect to the nozzle with the 45° mirror. The detector was then positioned for maximum signal and the diagnostic adjusted for zero differential signal between the beams. The arc heated hot diluent flow was then injected into the evacuated test section and the stability of the diagnostic was verified. Introduction of SF<sub>6</sub> (+O<sub>2</sub>) into the arc heater plenum resulted in the formation of F<sub>2</sub> near the walls. The F<sub>2</sub> concentration was then measured as a reduction in the probe beam intensity downstream of the walls.

The desired probe laser beam propagation contour along the 1-1/2 inch slit length is shown in Fig. 4a. The TEM<sub>00</sub> Gaussian intensity profile transverse to the beam propagation direction is shown in Fig. 4b. The beam contour boundaries thus correspond to the symmetric 1/e<sup>2</sup> peak intensity points of the Gaussian distribution and contain 86 percent of the beam power within them. The beam is focused so that the beam waist minimum, W<sub>02</sub>, occurs at the center of the slit nozzle length. For this condition, the probe beam waist maximum W' occurs at both ends of the slit nozzle.<sup>(5)</sup> W' and W<sub>02</sub> are related by the equation

$$W' = W_{02} \left[ 1 + \left[ \frac{Z' \lambda}{\pi (W_{02})^2} \right]^2 \right]^{1/2} \quad (2)$$

where Z' = 1.905 cm and λ = 0.325 x 10<sup>-4</sup> cm in this case. The focused beam waist may be related to the lens focal length F and the laser beam divergence (θ<sub>1</sub> = 0.20 x 10<sup>-3</sup> rad) by the approximate expression

$$W_{02} \approx F \theta_1 \quad (3)$$

to illustrate the relation between probe beam shape in the absorption region and lens focal length.

Fig. 5 is a plot of W' and W<sub>02</sub> versus lens focal length in the region of minimal achievable beam diameters. It is seen in the figure that the waist size near the slit nozzle ends reaches a minimum of W' = 5 x 10<sup>-3</sup> inch diameter for a ~ 9 inch focal length lens. The waist at slit nozzle center is even smaller at W<sub>02</sub> ~ 3.5 x 10<sup>-3</sup> inch diameter. This is the minimum beam end

$$z' = 0.750' \quad (1.095 \text{ CM})$$

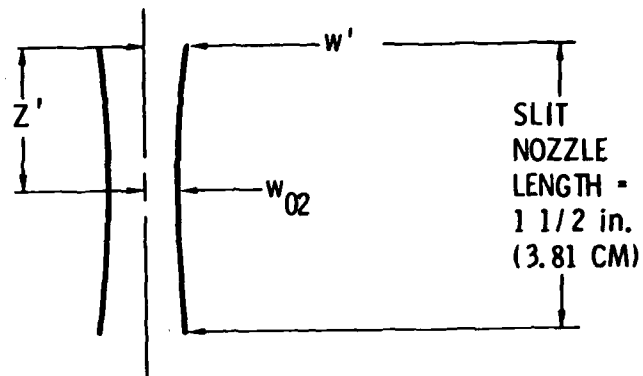


Fig. 4a. Probe laser beam geometry along slit nozzle length

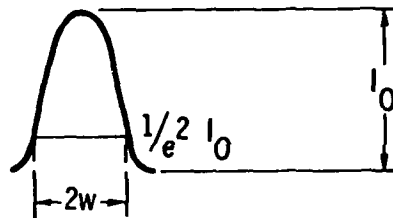


Fig. 4b.  $TEM_{00}$  Gaussian intensity profile transverse to propagation direction

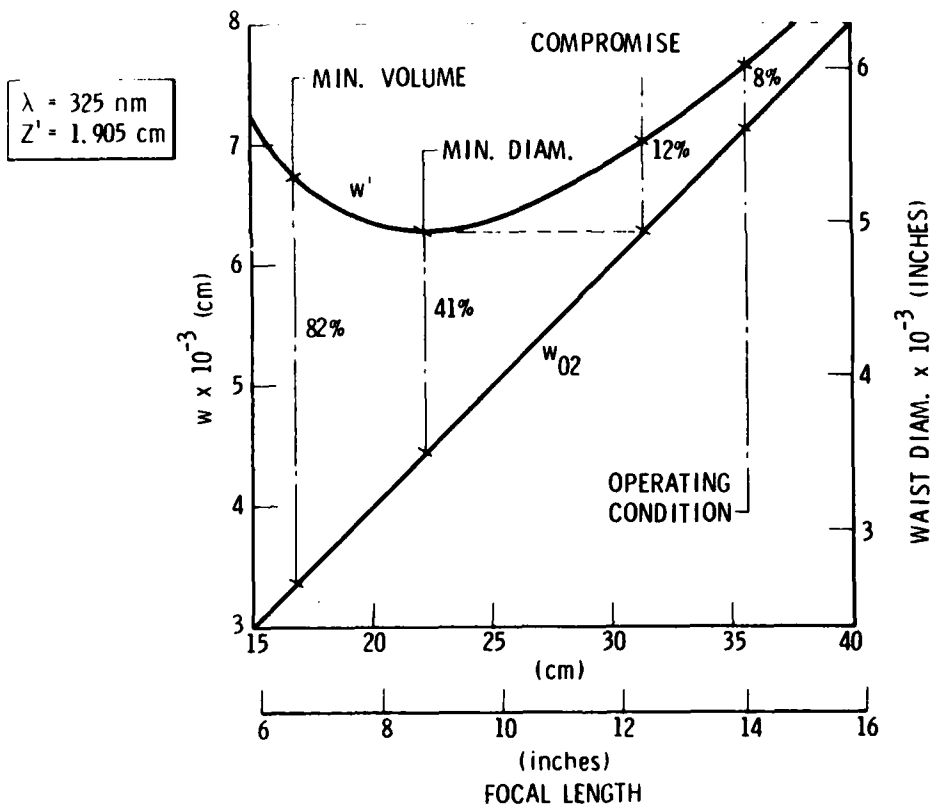


Fig. 5. Beam end waist,  $w'$  and beam center waist,  $w_{02}$  versus lens focal length

diameter that can be achieved for this experiment. However, the beam deviates somewhat from a cylindrical ideal in that the diameter of the ends is 41 percent greater than the center diameter. A closer approach to a cylindrical beam may be achieved but at the expense of increasing the beam diameter. A compromise between a small diameter beam and a small deviation from cylindrical shape may be achieved with the use of an ~ 12 inch focal length lens, as shown in the figure, which produces a center beam diameter equal to the minimum obtainable beam end diameter. Use of this lens produces a very nearly cylindrical beam with only 12 percent difference in nozzle center to end diameters. However, a longer focal length lens was required in this experiment to keep it outside the test section for ease of refined adjustment. The 14 inch focal length lens used in these experiments produced a 0.006 inch diameter beam with only 8 percent deviation from a cylindrical beam shape. Use of a 6.5 inch focal length lens results in a minimum volume probe beam, but with an 82 percent difference in nozzle center to end diameters. Lens position in the optical path must be precision calculated from well established laser divergence and lens focal length measurements to ensure accurate placement of the minimum beam waist at the slit nozzle center. See Ref. (5).

The slit nozzle array employed in these tests consisted of a set of linear slit nozzles with the dimensions 1-1/2 inch long by 0.200 inch center-to-center wide, and with a throat width equalling 0.010 inch, with secondary flow slit injection at the nozzle exits. A detail cross section drawing of the slit nozzle array is shown in Fig. 6. Arc-heated  $\text{SF}_6(+\text{O}_2)$  in He diluent provided the F atom flow for the nozzle array.  $\text{H}_2$  is injected along the trailing edges of the individual nozzles. See Fig. 7 for a photograph of the

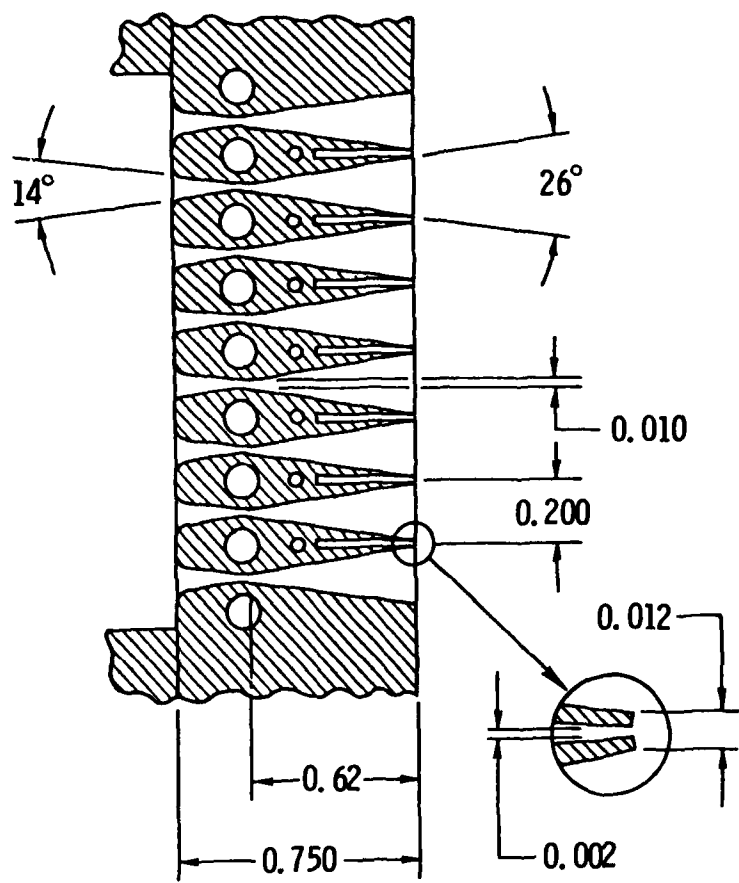


Fig. 6. Detail cross section drawing of slit nozzle array

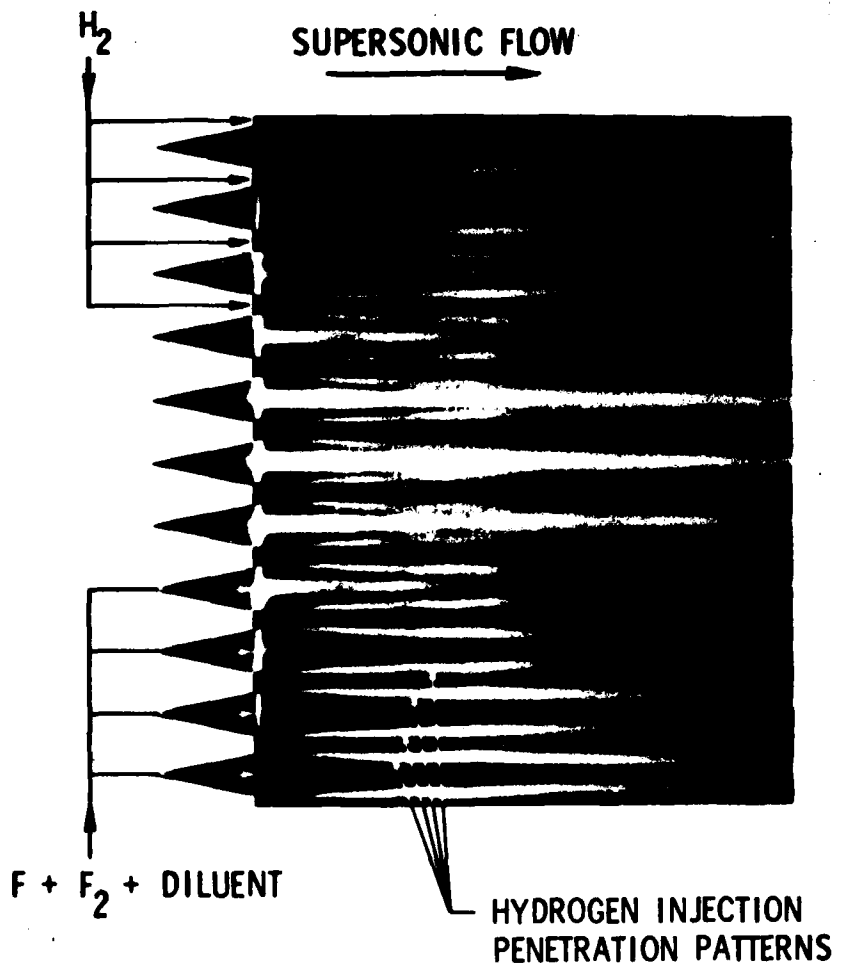


Fig. 7. Slit nozzle flow pattern

flow pattern from an array of these slit nozzles under conditions of H<sub>2</sub> injection into the hot flow. Note the laminar penetration pattern of the H<sub>2</sub> into the heated jet. The spreading rate was determined spectrographically by following the HF P<sub>1</sub>(6) line peak chemiluminescence. This measured penetration profile followed the relation  $\delta = 0.1 \sqrt{x}$ , in which x is the jet streamline dimension.

Flow conditions for these tests are listed in Table I where it is noted that the hot flow is principally helium. The cavity pressure was maintained at 4.5 Torr to achieve nominally matched jet conditions as determined by observation of the jet. This pressure ratio allows calculation of an adiabatic expansion helium flow Mach number of 4.3 and an equivalent area ratio of  $A/A^* = 6.7$ . The geometric area ratio is 19, which would yield a Mach number 6.4 flow if the nozzle were full. The equivalent area ratio is only  $\sim 1/3$  the geometric area ratio, indicating the presence of a thick viscous boundary layer. This inference is in agreement with the size of the central luminous patterns relative to the individual nozzle widths associated with each hot jet, as seen in Fig. 7. Pitot pressure profiles also indicate that the core flow is  $\sim 1/3$  of the nozzle flow width, i.e., each wall boundary layer is  $\sim 0.07$  inch thick.

TABLE I. Test Flow Conditions

Molar Flow Rates

SF <sub>6</sub>	6.8 millimoles/sec
O <sub>2</sub>	6.8 millimoles/sec
H <sub>2</sub>	350 millimoles/sec
He	625 millimoles/sec

Pressures

Plenum	600 Torr
Cavity	4.5 Torr

Temperature

Plenum	~ 2300 K
Cavity	~ 300 K

### III. RESULTS

Scanning of a single nozzle located near the center of eight 1-1/2 inch long slit nozzles was accomplished initially along a path 0.050 inch from the nozzle exit plane for conditions of (H<sub>2</sub>OFF) and (H<sub>2</sub>ON). The (H<sub>2</sub>OFF) scans indicated a peak F<sub>2</sub> absorption directly downstream of the H<sub>2</sub> injection slit reducing to zero at about 0.025 inch toward the nozzle centerline. The integrated absorption curve corresponded to a ~ 50 percent recombination of F atoms in the plenum for the test conditions. This measurement was confirmatory of previous bulk measurements on cooled copper nozzle flows.<sup>(3)</sup>

(H<sub>2</sub>ON) scans initially produced ambiguous results immediately downstream of the nozzle H<sub>2</sub> injection. This was demonstrated to be from probe-beam steering upon H<sub>2</sub> injection. This observation allowed determination of the H<sub>2</sub>-He penetration interface with no F or F<sub>2</sub> in the flow that corresponded to the penetration profile for F in the flow determined spectrographically by following the HF P<sub>1</sub>(6) line peak chemiluminescence. Inside this region (i.e., toward nozzle centerline) the F<sub>2</sub> absorption profile could be measured without this encumbrance and was determined to be similar to the (H<sub>2</sub>OFF) case; the exceptions are that the profile is slightly higher in peak height, ~10 percent to 20 percent narrower in width, and displaced toward the centerline a distance corresponding to the H<sub>2</sub> penetration distance. The H<sub>2</sub> injection essentially displaced the F<sub>2</sub> boundary layer inward and compressed it in the ~0.07 inch thick viscous boundary layer. Fig. 8 is a presentation of this data. The data point circles are scaled to represent the 0.006 inch diameter beam size; thus, the probe beam dimension relative to nozzle size, penetration

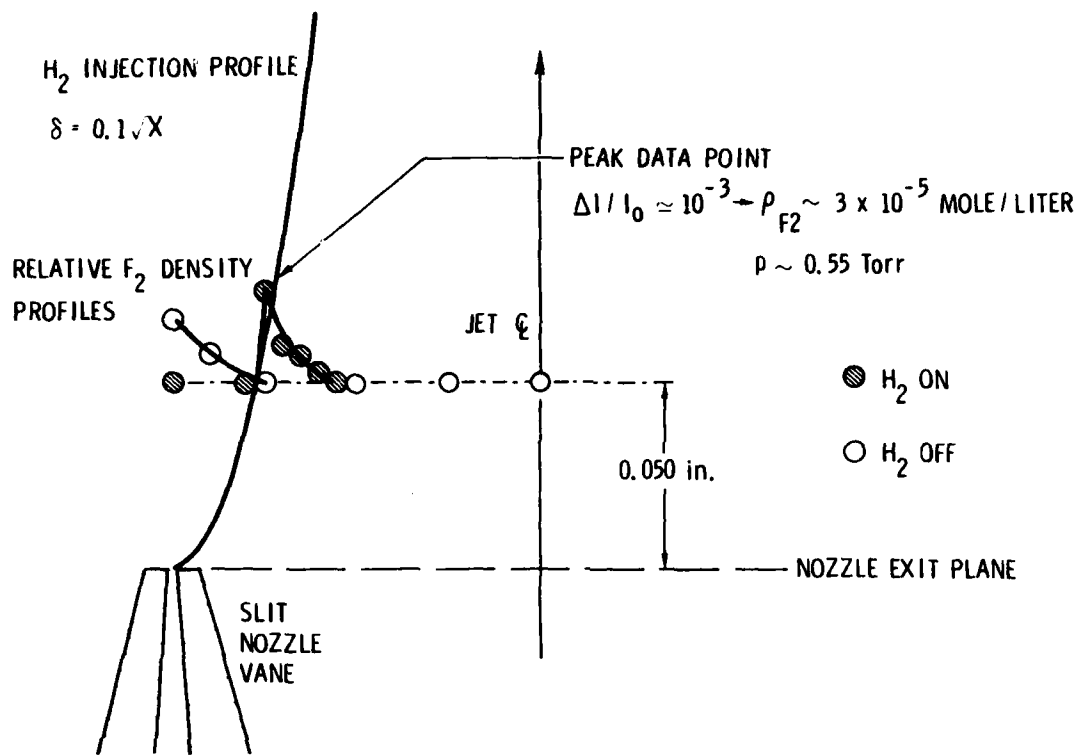


Fig. 8. Slit nozzle  $F_2$  absorption scan along 0.050 inch line for ( $H_2$ ON) and ( $H_2$ Off) conditions

profile width, and  $F_2$  boundary layer thickness can be inferred. The circles also cover the measurement uncertainties in both position ( $\pm 0.003$  inch) and signal intensity ( $\Delta I/I_0 \sim \pm 3 \times 10^{-5}$ ). The plot of data points is displaced 0.050 inch from the nozzle exit plane, which corresponds to the plane of measurement. The curves thus represent absorption values along the 0.050 inch line and should ideally be shown in three dimensions out of the plane of the drawing; however, they are folded back along the 0.050 inch line into the two dimensional representation in this figure.

The peak data point for the ( $H_2ON$ ) case was measured at  $\Delta I/I_0 = 10^{-3}$ , a factor 33 above the minimum signal observation level. This measurement corresponds to an  $F_2$  density of  $\sim 3 \times 10^{-5}$  mole/liter or a partial pressure of  $\sim 0.55$  Torr, i.e.  $\sim 1/10$  the flow static pressure.

A scan along a line 0.030 inch downstream of the nozzle exit plane was also performed for ( $H_2ON$ ) with results compatible with the 0.050 inch scan data. Data from the two scans are assembled in Fig. 9. The ( $H_2OFF$ ) points obtained in the  $\sim 0.050$  inch scan immediately downstream of the  $H_2$  injection slit have been translated in this presentation up to the nozzle exit plane as it is assumed that the profile would have this same shape in this region of no  $H_2$  flow. The relative  $F_2$  density profiles are presented as in Fig. 8. The viscous boundary layer profile, as inferred from pitot pressure measurements in the jets near the nozzle, is also presented in this figure to establish the relative sizes of the  $F_2$  and viscous boundary layers for this nozzle flow.

Measurements made near, and also 1 1/2 inches downstream from the nozzle exit plane transverse to both the flow and slit axis directions, indicated only  $\sim 15$  percent reduction in  $F_2$  flow concentration for the ( $H_2ON$ ) condition,

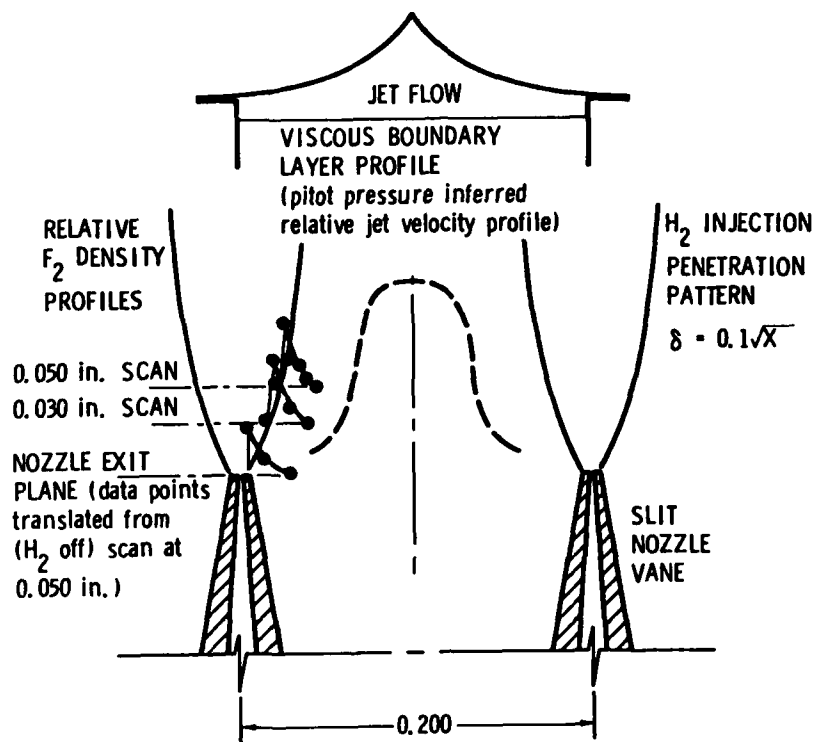


Fig. 9. Measured F<sub>2</sub> density profiles (relative units)

i.e.,  $\Delta I/I_0$  (near nozzle) =  $1.2 \times 10^{-4}$ ,  $\Delta I/I_0$  (1-1/2 inch downstream) =  $1.0 \times 10^{-4}$ . Thus the  $F_2$  passed through the laser gain region essentially unreacted. The low diffusion rate of  $F_2$  in He relative to  $H_2$  in He (factor ~ 0.23 smaller) would indicate that the  $F_2$  profile also passed through the laser gain region relatively intact and only slightly spread. The presence of mostly unreacted  $F_2$  downstream of the  $F + H_2$  reaction zone is consistent with the order of magnitude lower reaction rate of the  $H + F_2$ .<sup>(6)</sup> (However, this may not be the case for higher temperature and/or lower dilution level flows where hot reaction runaway may occur.)

#### IV. SUMMARY

A scanning  $F_2$  absorption diagnostic has been developed with a 0.006 inch diameter probe beam resolution over a 1-1/2 inch path length; the diagnostic has a 15 milli Torr  $F_2$  measurement sensitivity for scanning chemical laser slit nozzle flows in order to determine the  $F_2$  boundary layer profiles. The diagnostic was applied to a chemical laser nozzle flow and the  $F_2$  boundary layer was determined to be of exponential decay form with peak at the nozzle wall and of width  $\sim 1/3$  the viscous boundary layer. The  $F_2$  concentration profile was displaced inwardly by the  $H_2$  slit injection at the nozzle exit plane and apparently remained fairly intact in passing through the lasing zone. The principal deleterious effect of this  $F_2$  concentration in the flow derived from the attendant reduced F atom concentration. For the flow conditions under test, the presence of the  $F_2$  boundary layer had only a minor effect on  $H_2$  mixing with F atoms; a deleterious temperature rise, which could have been produced by the hot reaction ( $H + F_2$ ), did not develop.

## REFERENCES

1. Rushmore, W. L., F. B. Bossler, S. J. Andrysiak, T. Buddenhagen, W. F. Van Tassall, W. Chambers, W. Brandkamp and S. W. Zelazny, "CW HF and DF Chemical Lasers: Comparisons Between Theory and Experiment," Bell Aerospace Report No. 9500-920375, September 1980.
2. Hill, R. A. and P. J. Hargis, Jr., "Probes for Density Measurements of F<sub>2</sub>, HF and DF in Continuously Operating Chemical Lasers," Sandia Report No. 74-0432, January 1975.
3. Spencer, D. J., "Sensitive F<sub>2</sub> Absorption Diagnostic," Journal of Applied Physics 49 (7) July 1978, p. 3729-3732.
4. Spencer, D. J. and C. W. Clendening, Jr., "F<sub>2</sub> Absorption Measurement in a Combustion-driven Chemical Laser Nozzle," Journal of Applied Physics 49, (7) July 1978, p. 3733-3736.
5. For Gaussian beam calculations see for example A. E. Siegman, An Introduction to Lasers and Masers, McGraw-Hill, Inc. NY, 1971.
6. Cohen, N. and J. F. Bott, A Review of Rate Coefficients in the H<sub>2</sub>-F<sub>2</sub> Chemical Laser System, TR-0076(6603)-2, The Aerospace Corp., El Segundo, Calif., 15 April 1976.

## LABORATORY OPERATIONS

The Laboratory Operations of The Aerospace Corporation is conducting experimental and theoretical investigations necessary for the evaluation and application of scientific advances to new military space systems. Versatility and flexibility have been developed to a high degree by the laboratory personnel in dealing with the many problems encountered in the nation's rapidly developing space systems. Expertise in the latest scientific developments is vital to the accomplishment of tasks related to these problems. The laboratories that contribute to this research are:

Aerophysics Laboratory: Launch vehicle and reentry aerodynamics and heat transfer, propulsion chemistry and fluid mechanics, structural mechanics, flight dynamics; high-temperature thermomechanics, gas kinetics and radiation; research in environmental chemistry and contamination; cw and pulsed chemical laser development including chemical kinetics, spectroscopy, optical resonators and beam pointing, atmospheric propagation, laser effects and countermeasures.

Chemistry and Physics Laboratory: Atmospheric chemical reactions, atmospheric optics, light scattering, state-specific chemical reactions and radiation transport in rocket plumes, applied laser spectroscopy, laser chemistry, battery electrochemistry, space vacuum and radiation effects on materials, lubrication and surface phenomena, thermionic emission, photosensitive materials and detectors, atomic frequency standards, and bioenvironmental research and monitoring.

Electronics Research Laboratory: Microelectronics, GaAs low-noise and power devices, semiconductor lasers, electromagnetic and optical propagation phenomena, quantum electronics, laser communications, lidar, and electro-optics; communication sciences, applied electronics, semiconductor crystal and device physics, radiometric imaging; millimeter-wave and microwave technology.

Information Sciences Research Office: Program verification, program translation, performance-sensitive system design, distributed architectures for spaceborne computers, fault-tolerant computer systems, artificial intelligence, and microelectronics applications.

Materials Sciences Laboratory: Development of new materials: metal matrix composites, polymers, and new forms of carbon; component failure analysis and reliability; fracture mechanics and stress corrosion; evaluation of materials in space environment; materials performance in space transportation systems; analysis of systems vulnerability and survivability in enemy-induced environments.

Space Sciences Laboratory: Atmospheric and ionospheric physics, radiation from the atmosphere, density and composition of the upper atmosphere, aurorae and airglow; magnetospheric physics, cosmic rays, generation and propagation of plasma waves in the magnetosphere; solar physics, infrared astronomy; the effects of nuclear explosions, magnetic storms, and solar activity on the earth's atmosphere, ionosphere, and magnetosphere; the effects of optical, electromagnetic, and particulate radiations in space on space systems.

5-83

DTIC